Electronic Supplementary Material (ESI) for Analytical Methods.
This journal is © The Royal Society of Chemistry 2019

Influence of TiO_2 and ZrO_2 nanoparticles deposition on Stainless Steel furnace used for trace element determination by TS-FF-AAS.

G. Carrone[*a], D. Onna[*b], E. Morzan[c], R. Candal[a], Y.S. Minaberry[d], J. Schneider[d], M. Tudino[d]

[a.] *Instituto de Investigación e Ingeniería Ambiental, CONICET, Universidad Nacional de San Martin, Campus Miguelete, 25 de Mayo y Francia, 1650, San Martin, Provincia de Buenos Aires, Argentina.*
[b.] *Instituto de Nanosistemas, CONICET, Universidad Nacional de San Martin, 1650, San Martin, Buenos Aires, Argentina.*
[c.] *Comisión Nacional de Energía Atómica, General Paz 1499, Buenos Aires, B1950KNA, Argentina.*
[d.] *Laboratorio de Trazas, DQIAQF, Facultad de Ciencias Exactas y Naturales, Universidad de Buenos Aires, Ciudad Universitaria Pab. II, C1428EHA, Buenos Aires, Argentina.*
E-mail: carroneguillermo@gmail.com, diego.onna@qi.fcen.uba.ar

S1. EDS RESULTS

Table S1. Atomic composition of the samples determined by energy dispersive x-ray spectroscopy (EDS).

	Average Weight %		
Element	Bare Steel	TiO_2@Steel	ZrO_2@Steel
C K	3.76	4.04	4.19
O K	29.76	26.08	26.56
Cr K	2.40	1.47	1.99
Mn K	1.44	0.54	2.31
Fe K	62.26	61.80	61.54
Ni K	0.38	0.15	0.94
Ti K	-	5.92	-
Zr L	-	-	2.46

S2. COMPARISON OF LODs.

Table S2 shows the LOD (limit of detection) of Ag, Cd, Pb and Se, using bare steel, TiO2@Steel, ZrO2@Steel and Ni furnaces, and compared with LODs presented in literature.[1]

Table S2. Limit of detection (3s) for Ag, Cd, Pb and Se found for different furnaces (expressed in $\mu g.L^{-1}$)

Analyte	Bare Steel	TiO2@Steel	ZrO2@Steel	Ni tube	Ni tube[1]
Ag	9	7	7	2.6	0.6
Cd	5	0.5	0.4	0.3	0.3
Pb	22	4	7	9.1	2.4
Se	96	71	92	317	310

S3. FURNACE TEMPERATURE DETERMINATION

Images were taken using a digital camera in order to determinate the furnace temperature. Three furnaces, bare steel, ZrO_2@Steel and TiO_2@Steel, were analysed at different injection flow rate. Figure S1 shows RGB images (left) and false colour images (right) of ZrO_2@Steel furnace at injection flow rates between 0 and 1.9 mL.min^{-1}. The false colour images depict the temperature calculated using the green channel. All furnaces presented the same behaviour, increasing the injection flow rate decreases the temperature in the injection region. Figure S2 shows plots of the temperature measured in the horizontal line shown in Figure S1, for the three types of furnaces. In particular, (i) the bare steel furnace exhibits the highest temperature at injection flow rate of 0 mL.min^{-1} and presents the highest decrease in temperature cause by injecting the sample. (ii) The ZrO_2@Steel shows an opposite behaviour, the lowest temperature and the lowest decrease in temperature. (iii) The TiO_2@Steel, the coatings behaviour is between ZrO_2@Steel and bare steel. Figure S3 shows how the internal and external surface of the furnace change their temperature by increasing the injection flow rate. When there is no flow, a temperature gradient between the external temperature (a) and the inner temperature (b) is established due to the thermal conductivity of the material. Then, when a sample enters into the furnace with a certain flow rate and is vaporized, a decrease of the temperature at the inner surface occurs (c) and, at the same time, the external surface decrease its temperature as some energy is consumed for vaporizing the sample (d). While increasing the injection flow rate (1<2<3<4, arrows), a higher decrease in temperature is observed. As shown in the scheme, the decrease in temperature is greater in the case of bare steel than for coated furnace.

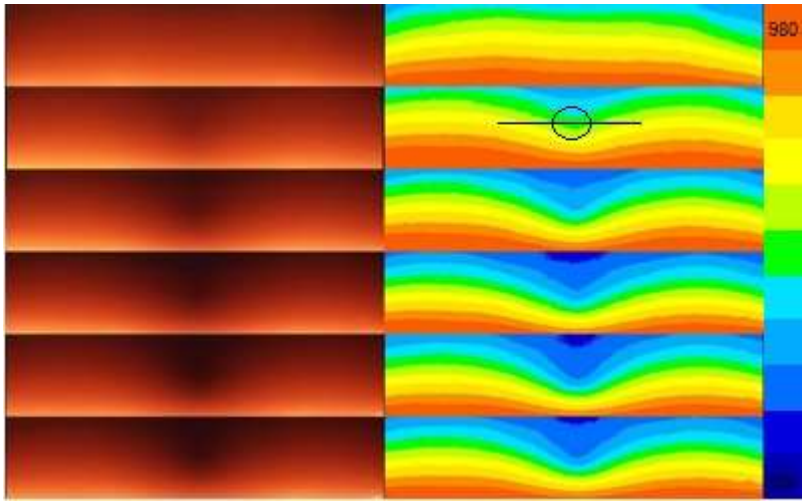

Figure S1. RGB images (left) and false colour images which represents temperature (right) of ZrO_2@Steel furnace at different flow rates (0, 0.6, 0.8, 1.3, 1.7 and 1.9 mL.min^{-1} from top to bottom).

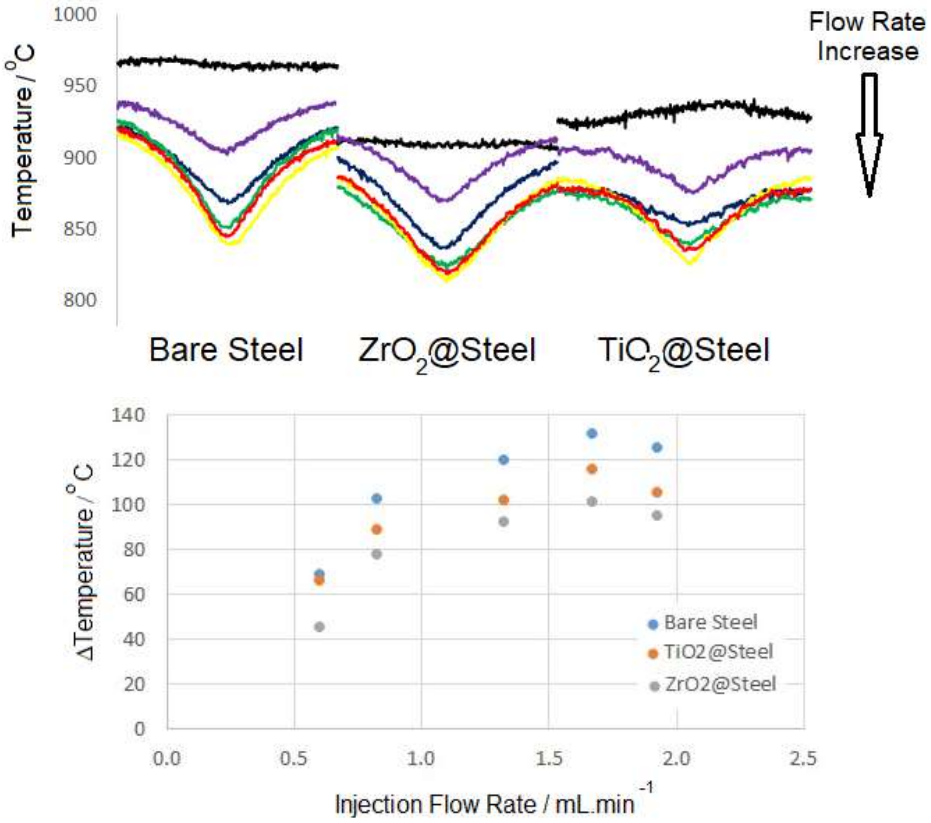

Figure S2. Top: Furnace temperature obtained on a horizontal line that pass through the injection region, for different furnaces while increasing the injection flow rate (black, 0; violet, 0.6; blue, 0.8; green, 1.3; yellow, 1.7; red, 1.9 mL.min^{-1}). The sampling region is indicated by a line in Figure S1. Bottom: Difference between the minimum temperature at different injection flow rates and the temperature with no flow.

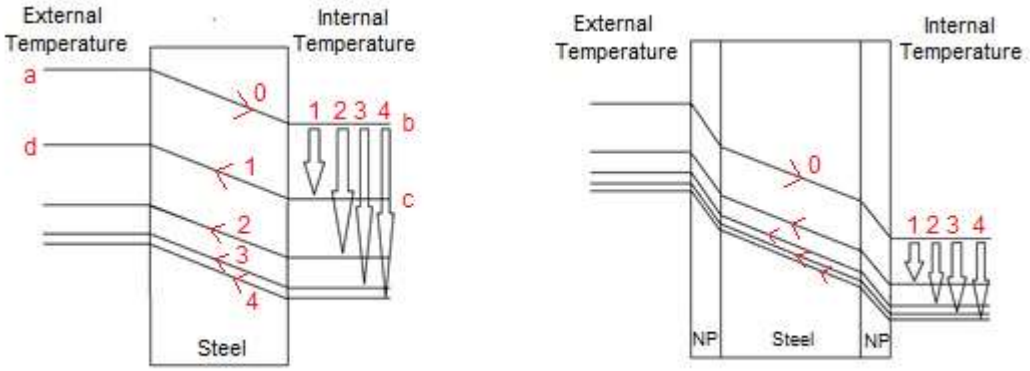

Figure S3. Scheme representing external an internal temperature of the furnace (uncoated, left; coated, right). Arrows represent the decrease of temperature generated when sample is atomized, this decrease is higher while increasing the sample injection flow rate (1<2<3<4). NOTE: as the thermal conductivity is lower for the ceramic material, the temperature difference across the material is higher.

It is worth noticing that the sample injection region was considered as a circle of 8.750 mm (175 pixels) diameter, centred at the opposite site of the injection capillary (circle shown in Figure S1). This length (8.750 mm) is the standard deviation (σ) of the normalized curves (shown in Figure S4) obtained of plots shown in Figure S2.

The thermal spatial distribution of bare steel and ZrO_2@Steel furnaces were obtained for different injection flow rates. The histograms of the temperature at the sample injection region (circle of 8.750 mm) are shown in Figure S5. The ZrO_2@Steel distribution are narrower and the medians for different injection flow rates are closer, indicating a more homogeneous thermal distribution. Also, the furnace temperature variation, between a certain injection flow rate and no flow, was represented with false colour images in Figure S6. The ZrO_2@Steel (right) exhibits a more homogeneous thermal distribution, as discussed before.

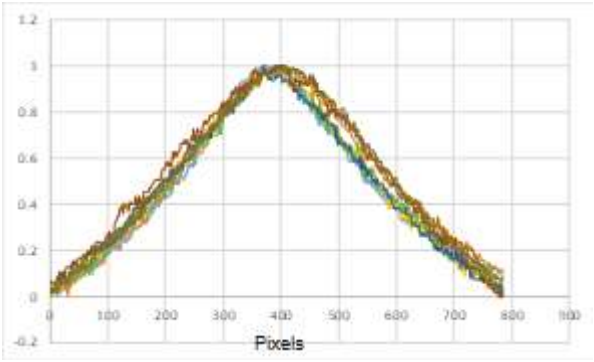

Figure S4. Normalized furnace temperature obtained on a horizontal line that pass through the injection region, for bare steel and ZrO_2@Steel furnaces while increasing the injection flow rate

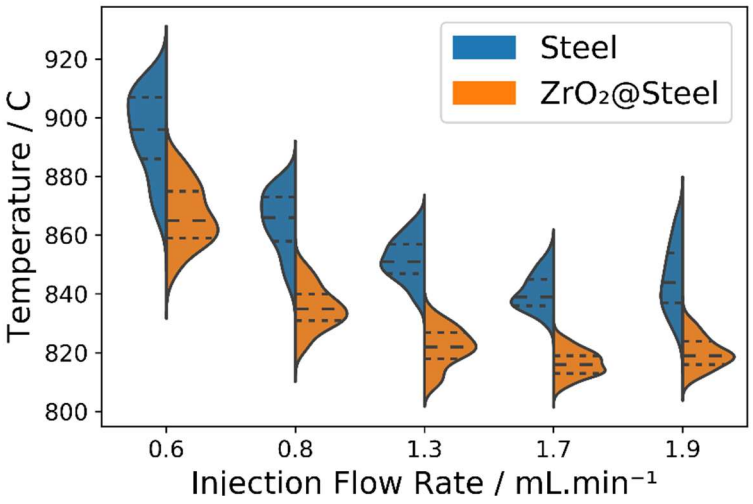

Figure S5. Violin plot of the thermal spatial distribution in sample injection region, at different flow rates for bare steel (blue) and ZrO_2@Steel (orange) furnace. The median and quartiles are indicated with dashed lines. The sampling region is indicated by a circle in Figure S1.

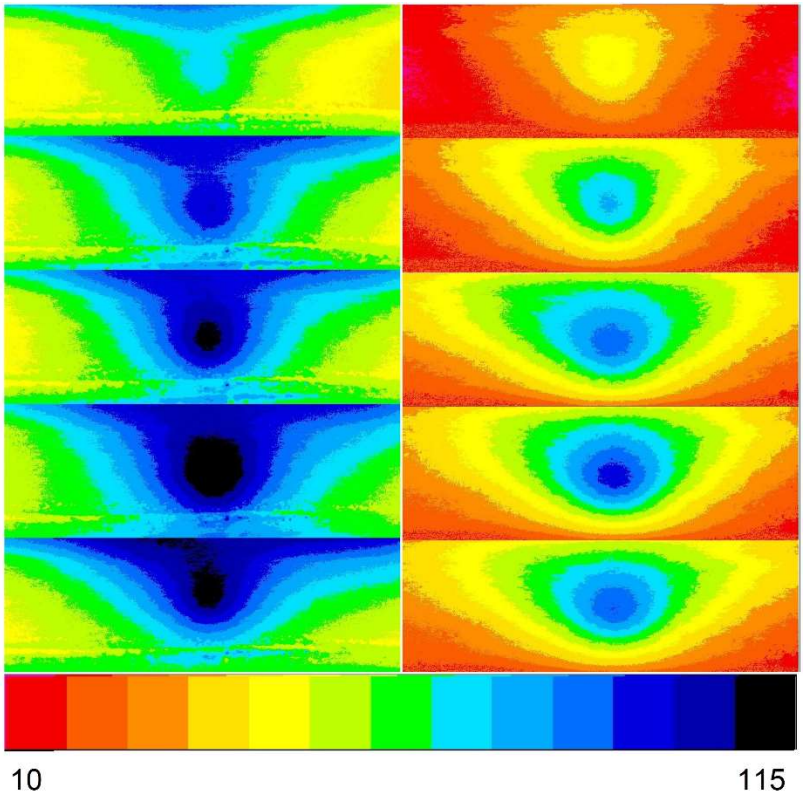

Figure S6. False colour images representing decrease of temperature, for the bare Steel furnace (left) and the ZrO2@Steel furnace (right), between no injection and different flow rates (0.6, 0.8, 1.3, 1.7 and 1.9 mL.min^{-1} from top to bottom).

The temperature of the coated furnaces is lower than the bare steel ones (Figure S2), indicating that the ceramic coatings could be reflecting the IR irradiation from the air-acetylene flame.[2] Then, the NPs coatings could act as a cool coatings[3] and less heat is transferred to the steel. In general, the lower temperature is associated with a hindrance to the analytical signal. Nevertheless, this signal improves at the coated furnaces. The thermal distribution is more homogeneous on the coated furnaces (Figure S4), probably produce by a bigger desolvation zone.[4] In the case of the coated furnaces, the wettability and rugosity caused by the NPs might led to a lower splashed angle,[5] increasing the desolvation region. Also, it is possible that the improvement at the vaporization would improve the analyte availability for atomization, producing a higher analytical signal (Figure 2, maintext). In addition, a surface-analyte interaction could be catalysing the analyte atomization (eg. Pb to Se exhibits greater signal for TiO_2@Steel than ZrO_2@Steel, even though this last one presents more homogeneous thermal distribution).

S4. ANALYTICAL SIGNAL WHEN INCREASING SAMPLE FLOW RATE.

Figure S7 shows the percentage variation of the analytical signal when increasing the sample injection flow rate for Cd, Pb, Ag and Se.

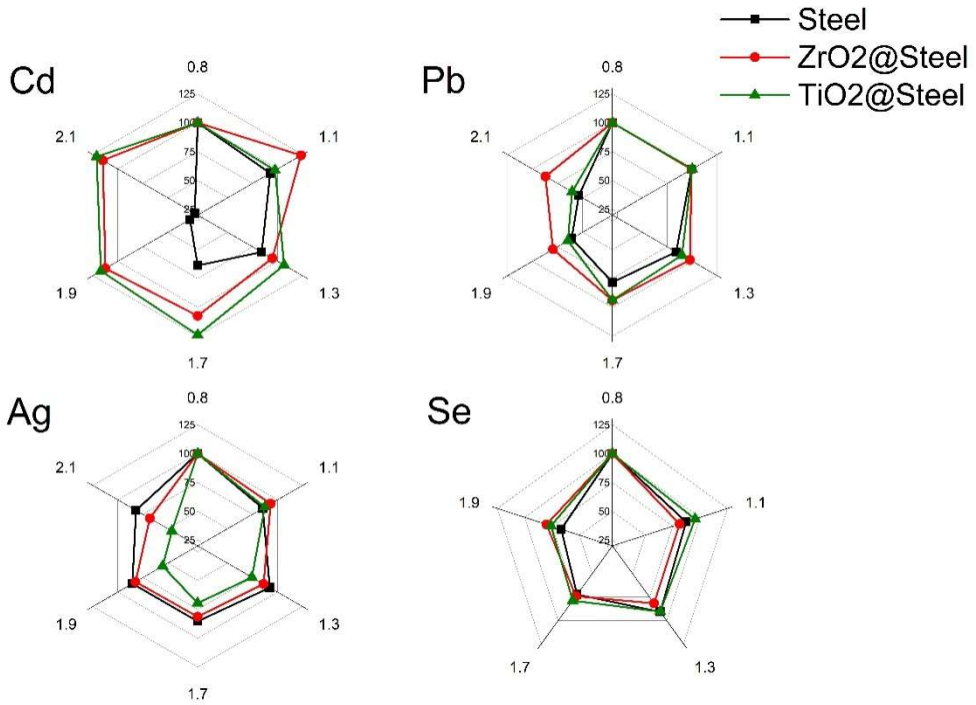

Figure S7. Percentage variation of the analytical signal by increasing the simple injection flow rate (ml.min^{-1}), obtained for each analyte respect to the flow rate where the analytical signal is maximum (0.8 mL.min^{-1}, for all cases).

S5. IMPROVEMENT FOR Cu DETERMINATION.

Figure S8 shows the analytical response of solutions containing Cu, using bare steel and TiO_2@Steel furnaces. An increment of 100% in the analytical sensitivity is observed for the coated furnace compared to the bare steel one.

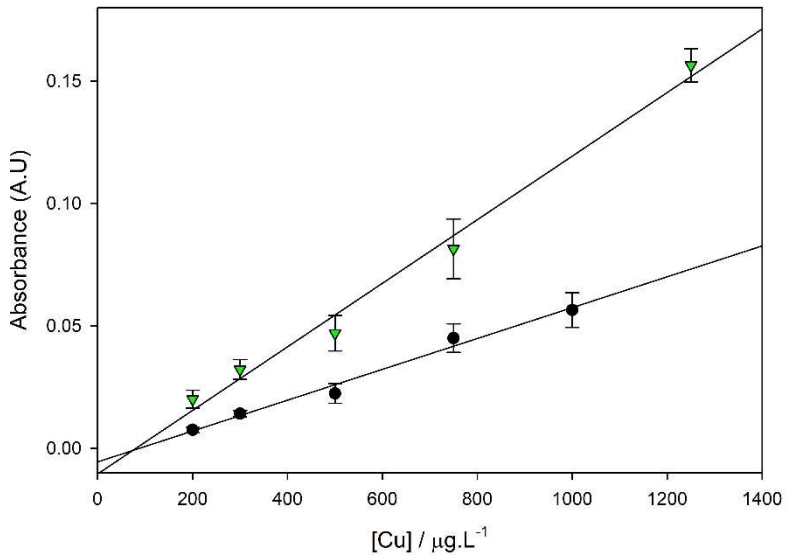

Figure S8. Analytical response of Cu solutions using furnace of bare stainless steel (black) and TiO_2@Steel (green).

S5. FURNACE LIFETIME AND REUSABILITY

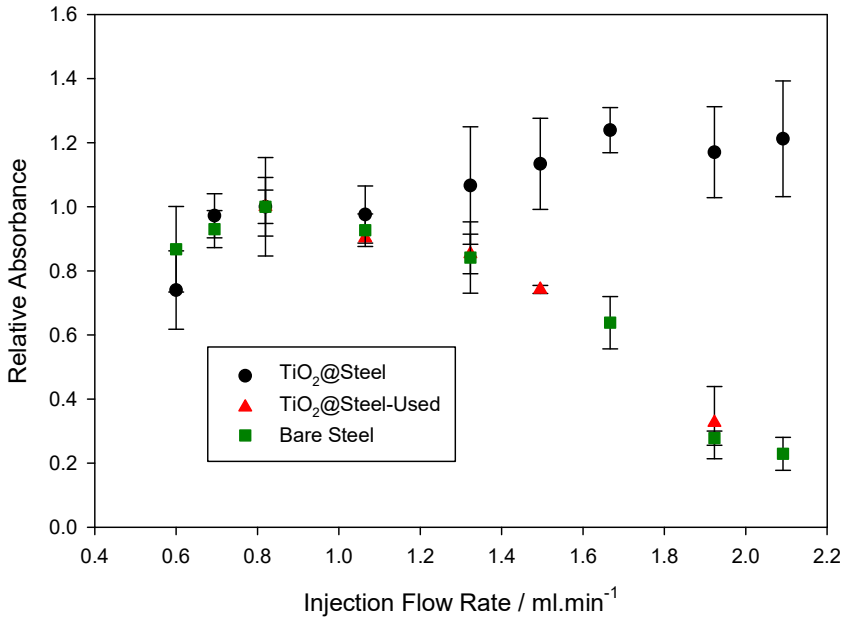

Figure S9. Analytical response of Cd, at 100 μg.L^{-1} level, at different sample injection flow rate, using furnace of bare stainless steel (green), TiO_2@steel (black) and TiO_2@steel used after cooling (green). NOTE: Values represent relative absorbance compared to 0.8 mL.min^{-1} flow rate signal (maximum response in bare steel furnace).

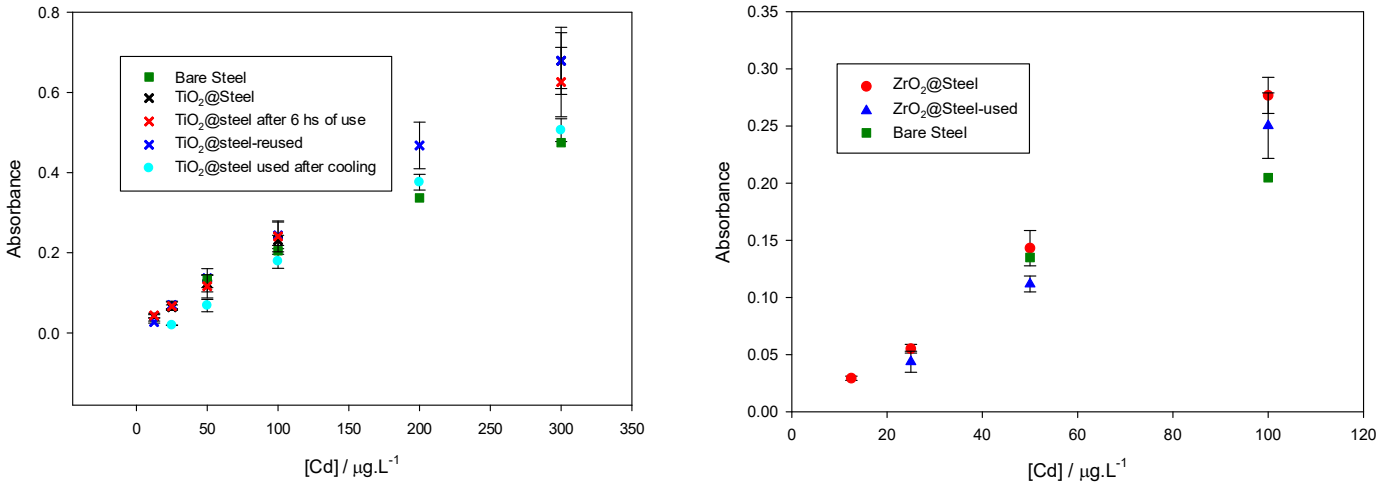

Figure S10. Left: Analytical response of solutions containing Cd, at 0.8 ml.min^{-1} flow rate using furnace of bare stainless steel (green square), TiO_2@steel (black cross), TiO_2@steel-reused (blue cross), TiO_2@steel after 6 hs of use (red cross) and TiO_2@steel used after cooling (light blue circle). Right: Analytical response of solutions containing Cd, at 0.8 ml.min^{-1} flow rate using furnace of bare stainless steel (green square), ZrO_2@steel (red circle), ZrO_2@steelused after cooling (blue triangle).

REFERENCES

1. J. Davies and H. Berndt, *Anal. Chim. Acta*, 2003, **479**, 215.
2. a) V. C. Malshe and A. K. Bendiganavale, *Recent Pat Chem Eng*, 2008, ***1*(1)**, 67. b) D. A. Brennan, I. Mabbett, J. Elvins, N. P. Lavery and D. A. Worsley, *Eur J Comp Mech*, 2016, **25(3)**, 294.
3. C. J. Chung, H. I Lin, H. K. Tsou, Z. Y. Shi and J. L. He, *J Biomed Mater Res B*, 2008, **85(1)**, 220.
4. E. Morzan, J. Stripeikis and M. Tudino, *Anal Chem Res*, 2015, **4**, 1.
5. S. H. Kim, Y. Jiang and H. Kim, *Exp Therm Fluid Sci*, 2018, **99**, 85. b) H. Kim, B. Truong, J. Buongiorno and L. W. Hu, *J Therm Sci Tech-Jpn*, 2012, **7(3)**, 453. c) J. D. Bernardin and I. Mudawar, *J Heat Transf*, 1999, **121(4)**, 894. d) G. Liang, and I. Mudawar, *Int J Heat Mass Tran*, 2017, **106**, 103.